Available online at www.sciencedirect.com
SCIENCE DIRECT®
Journal of Crystal Growth 269 (2004) 432–442
JOURNAL OF CRYSTAL GROWTH
www.elsevier.com/locate/jcrysgro

# Characterization of bulk AlN with low oxygen content

M. Bickermann*, B.M. Epelbaum, A. Winnacker

*Department of Materials Science 6, University of Erlangen-Nürnberg, Martensstr. 7, D-91058 Erlangen, Germany*

Received 13 October 2003; accepted 14 May 2004

Communicated by D.W. Shaw

**Abstract**

We have established a PVT growth process for preparation of polycrystalline bulk AlN with low impurity content, especially in regard to oxygen. With this process at hand, we compare crystals grown at different temperatures in order to investigate the impact of growth temperature on impurity incorporation and crystal properties. Bulk AlN samples grown at temperatures of 2125°C and 2225°C were investigated. Chemical analysis shows that oxygen contamination in the crystals equals to a concentration of about $1 \times 10^{19}\,\mathrm{cm}^{-3}$ near the final as-grown surface. This is the lowest value in bulk AlN reported up to date. No change of oxygen contamination with growth temperature is observed. The samples are electrically insulating at room temperature. Resistivity measurements on a sample grown at 2225°C showed a thermal activation energy of about 860 meV in the 500–650 K range. In optical absorption, a band at around 2.8 eV was detected in all of our samples, while different absorption bands show up in the 3.0–6.0 eV energy range. The bands are presumably 'oxygen-related', but as changes in growth temperature lead to significant variation in the optical properties of AlN even in samples with comparable oxygen content, we suggest that these bands are also influenced by temperature-dependent formation of intrinsic defects. Additional bands at 5.0 and at 5.6 eV, which are observed only in samples grown at lower temperatures, are attributed to the presence of nitrogen vacancies. Finally, thermal conductivity $\lambda$ of the samples was found to be mainly limited by phonon–phonon scattering in the investigated temperature range of $T = 293-1473\,\mathrm{K}$. In the resulting relation $\lambda \propto \beta/T$, the variation of $\beta$ is caused by scattering on aluminum vacancies and reflects differences in growth temperature as well as sample position. Presumably, aluminum vacancy formation does not only depend on oxygen contamination, but also on growth temperature. We conclude that although further reduction of oxygen contamination is considered a key prerequisite for enhancing crystal quality, variations in optical, electrical, and thermal properties, as observed in samples grown at different temperatures, can be attributed to vacancy formation rather than to oxygen alone. Thus, vacancy formation control is another key issue for further optimization in AlN bulk crystal growth.
© 2004 Elsevier B.V. All rights reserved.

*PACS:* 61.72.Ji; 61.72.Ss; 65.40.−b; 78.40.Fy; 81.05.Ea; 81.10.Bk

*Keywords:* A1.Impurities; A1.Point defects; A2.Growth from vapor; B1.Nitrides; B2.Semiconducting aluminum compounds

*Corresponding author. Tel.: +4991318527730; fax: +4991318528495.
*E-mail address:* matthias.bickermann@ww.uni-erlangen.de (M. Bickermann).

0022-0248/$ - see front matter © 2004 Elsevier B.V. All rights reserved.
doi:10.1016/j.jcrysgro.2004.05.071

## 1. Introduction

Recent major developments in GaN semiconductor and optoelectronics technology have driven much interest toward aluminum nitride (AlN) and gallium nitride (GaN) bulk crystals, which are considered ideal substrates for III-nitride epitaxy. Up to now the potential of these materials in substrate applications has been disadvantaged by a lack of sufficiently large and perfect single crystals. In this context, preparation of AlN crystals by physical vapor transport (PVT) seems to be very promising.

Since the pioneering work of Slack and McNelly [1,2], a number of crystal growth studies on AlN [3–7] have been published, mainly aiming toward increasing the size of AlN single crystals. However, the role of impurity incorporation and vacancy formation during sublimation-recondensation (PVT) growth of bulk AlN crystals has been paid little attention till now. According to Slack et al. [1,2,8], oxygen is the most common impurity in semiconductor nitrides. Oxygen contamination is known to negatively influence crystal properties (e.g. electrical and optical properties, thermal conductivity) as well as structural quality [8–10]. The system Al–O–N can form solid oxynitride $(AlN)_m(Al_2O_3)$ compounds [11–16] at temperatures in the range of 1000–2050°C. Influence of other impurities and intrinsic defects on structural and electrical properties of bulk AlN is also predicted by theoretical calculations [2,17–20]. However, up to now experimental data is limited to AlN layers exhibiting a high number of structural defects [21,22].

We have established a PVT growth process for the preparation of polycrystalline bulk AlN with low impurity content, especially in regard to oxygen. With this process at hand, we compare crystals grown at two different temperatures in order to investigate the impact of growth temperature on impurity incorporation and crystal properties. The main research targets were (i) to see if and how the crystal properties resulting from the growth process fit to previously published data on bulk AlN, and (ii) to investigate the potential of growth temperature adjustment as well as further reduction of impurity incorporation as accomplished by our growth process in order to further improve electrical and optical characteristics of the bulk material.

## 2. Growth process

AlN crystal growth was accomplished by sublimation of an AlN charge placed in the hot zone of the tungsten crucible and subsequent condensation of vapor species in a cooler region as shown in Fig. 1. Our growth process was very similar to that described by Slack and McNelly [1,2]. Two deviations from the procedure of Slack and McNelly were (i) vertical positioning of the growth crucible (similar to well-established growth of SiC crystals by sublimation [23]) and (ii) use of two independently controlled heating zones.

The starting material was AlN powder containing about 0.6 %wt of oxygen supplied by Chempur AG, Germany. Prior to the use for crystal growth, commercially available AlN powder was resublimed in the same growth furnace shown in Fig. 1 in the atmosphere of high-purity nitrogen but under stronger temperature gradient. Before resublimation, adsorbed oxygen and moisture was removed by heating under high vacuum ($10^{-7}$ mbar). During resublimation the powder was kept at about 2325°C and crucible lid where

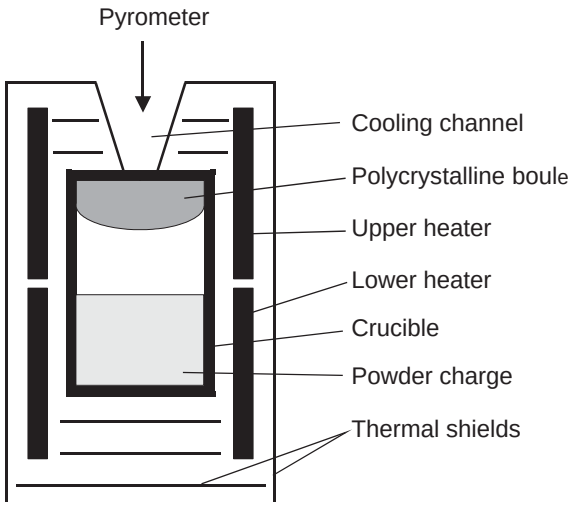


Fig. 1. Schematic drawing of the growth setup.

the material was condensed at about 2100°C. The charge of 200 g was normally completely resublimed during 24 h of holding time. The sublimation product collected on the crucible lid comprised two very different portions: a white layer produced by small crystals of micrometer size and generated in the beginning of sublimation transport process was followed by brown colored dense polycrystalline mass consisting of imperfect crystals up to 3–5 mm in size as shown in Fig. 2.

The white layer product is identified by powder XRD analysis as a mixture of AlN (PDF card ♯25-1133) and cubic $Al_3O_3N$ (PDF card ♯36-0050, see also Ref.[16]). We estimate the $Al_3O_3N$ content in the mixture from XRD measurements to be below 1 mol%. White layer formation starts at temperatures as low as 1300°C, but most of the layer was formed at 1700–1900°C presumably because of $Al_2O_3$ decomposition in nitrogen leading to volatilization of aluminum in the form of $Al_2O$ [24]. Condensation of $Al_2O$ in excess of nitrogen on the colder crucible lid yields rather fine particles of AlN and $Al_3O_3N$ with diameters of about 2–5 μm since at this temperature atomic surface mobility is too low to produce larger crystals.

After oxygen in the system is exhausted, this reaction-induced process stops. Transport starts again at temperatures above 2000°C due to evaporation of pure AlN in PVT process, leading to condensation of brownish crystals of AlN with pronounced grain selection as shown in Fig. 2. The white $AlN/Al_3O_3N$ layer was mechanically removed from the main portion of resublimed bulk product, which was used for the subsequent growth process.

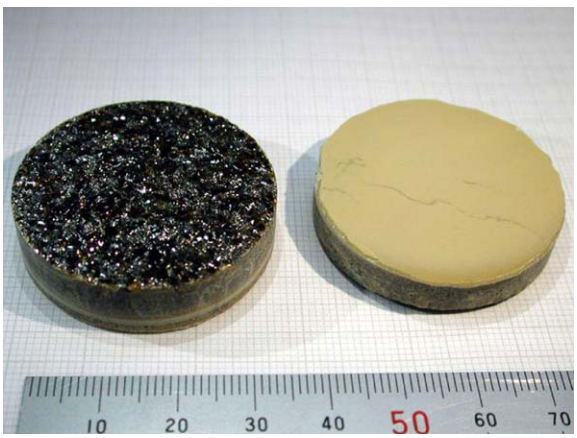


Fig. 2. Resublimed AlN starting material (round-grinded boules, each 37 mm in diameter). The boule on the left is shown from the final as-grown surface, the boule on the right is turned upside down and shows the white $AlN/Al_3O_3N$ layer.

In the growth process, the charge of about 200 g was placed in the bottom part of tungsten crucible. Two series of growth experiments were made in which the growth temperature on the crucible lid was set to 2125°C (series A) and 2225°C (series B). In all experiments source temperature was 50–75°C higher than the growth temperature. The furnace was operated in high-purity $N_2$ gas at pressure below 1000 mbar. Holding time was 12–36 h depending on temperature range. During this growth period, a polycrystalline, dense boule of 2 in in diameter and up to 10 mm in height was produced.

Polycrystalline samples of both series A and B show inhomogeneities because the grains in the boules exhibit different defect densities as well as different coloration and optical transmission. Nevertheless, there are significant differences in the general appearance between samples from series A and B. Bulk samples from series A (grown at lower temperature) are light yellow in color and translucent, whereas high-temperature samples from series B are brown and partially non-transparent in particular because of grain boundaries decoration. The growth surface of samples from series A is built mainly of well-developed hexagonal (0 0 1) as well as rhombohedral (1 0 2) and (1 0 1) faces, see Fig. 3 (left), but the size of the crystallites is always less than 2 mm. Samples from series B show a less regular growth surface, but single crystallites were as big as 5 mm × 3 mm, as shown in Fig. 3 (right). From the samples of both series cylindrical pieces 12 mm in diameter parallel to growth direction were drilled and subsequently cut into wafers of 0.8 mm thickness.

## 3. Impurity content

Impurity content was determined by glow discharge mass spectrometry (GDMS) on polycrystalline rods $2 \times 2 \times 20\,mm^3$ in size, cut from

near the final as-grown surface of ingots from both series A and B. The measured concentrations are listed in Table 1. Additionally, spark source mass spectrometry (SSMS) was performed on four polycrystalline rods, each $3 \times 3 \times 16\,mm^3$ in size, cut from the middle part of an ingot from series B. The maximum impurity content in commercial AlN powder used as starting material, as specified by the manufacturer, is 6000 ppm wt of oxygen, 300 ppm wt of carbon, 20 ppm wt of iron and 500 ppm of other metals including Al.

Comparing these values with Table 1 shows that the concentrations of oxygen and metal impurities decrease by almost two orders of magnitude as the starting material is finally transformed into bulk crystals. During the resublimation process (cf. Section 2), most impurities become volatile and are removed from the crucible. Additionally, segregation should take place and remaining impurities, e.g. transition metals, are repelled from the growth interface. Thus, most impurities are present in the boule only at sub-ppm levels. It may be possible that an initial growth layer is contaminated with oxygen and other impurities at higher values as compared to the measured samples. As most impurity sources are finite at growth conditions, contamination is expected to decrease as growth proceeds.

Fig. 3. Samples (round-grinded, each 12.5 mm in diameter, about 1 mm in height) cut from polycrystalline AlN boules grown at temperatures of 2125°C (series A, left figure) and 2225°C (series B, right figure). The sample's surfaces show the final as-grown surfaces of the respective boules.

Following Table 1, incorporation of most impurities—with the exception of Cr, Fe, and Ni, for which post-growth contamination by sample machining cannot be fully excluded—seems to be enhanced at higher growth temperatures. We attribute this to enhanced volatilization of impurities in the colder areas of the growth chamber with increasing temperature, as the resublimation process was the same for both series. As the dominating impurities, carbon and oxygen, are light-weight and difficult to detect by GDMS, additional samples from series B were investigated by SSMS, resulting in values of $105 \pm 30$ ppm wt for carbon and $145 \pm 67$ ppm wt for oxygen. Within the error range the SSMS values correspond well with the GDMS values.

The fabricated AlN crystals have the lowest oxygen content reported up to date for bulk AlN. Oxygen contamination as measured by GDMS analysis in the ingot from series B equals to a concentration of about $1 \times 10^{19}\,cm^{-3}$. As the samples from both series yield comparable results, oxygen incorporation obviously does not depend significantly on growth temperature in the investigated temperature range. However, the measurement accuracy in the case of oxygen is rather low.

In order to investigate if contamination with carbon and oxygen leads to formation of compounds other than AlN within the boules, X-ray diffraction (XRD) was performed using a Panalytical X-Pert system with Cu–K$\alpha$ radiation equipped with $\Theta/\Theta$ beam geometry, multi-line detector and variable focus. Regardless of sample position (i.e. from the first grown layer to the final

Table 1
Chemical analysis (GDMS) of impurities in grown AlN boules (all values in ppm wt)

| Series | Growth temperature °C | C | O | W | Na | Si | Ti | Cr | Fe | Ni | Zn | S | As | P |
|---|---|---|---|---|---|---|---|---|---|---|---|---|---|---|
| A | 2150 | ~100 | ~100 | 1.0 | 0.07 | 2.0 | 0.92 | 0.40 | 1.3 | 0.20 | <0.05 | 0.53 | <0.01 | 0.03 |
| B | 2250 | ~100 | ~86 | 7.9 | 7.3 | 2.5 | 2.5 | <0.2 | 0.15 | <0.05 | 0.12 | 1.3 | 0.23 | 0.56 |

as-grown surface of the boule) and origin (series A or B), some spectra show a complex structure of very small peaks, while others do not. Note that the intensities of these peaks are about two orders of magnitude lower than adjacent AlN peaks. We were able to identify crystalline compounds from these peaks in some cases; in general, however, not all peaks could be assigned.

Abundance of $\alpha$-$Al_2O_3$ strongly textured along *a*-axis was detected on a polished wafer from series B, but a quantitative analysis was not possible because of the texture. In some of the XRD spectra of crushed samples from both series A and B, traces of oxynitride compounds of the type $(AlN)_m(Al_2O_3)$ were identified (see also Refs. [13,15]). No peaks related to tungsten or carbon were observed.

Although traces of oxygen-containing compounds are present in some of our samples, most of the oxygen should be present as atomic impurity in the AlN crystals. This corresponds with the fact that the reported oxygen solubility limit in AlN exceeds $9 \times 10^{20}\,cm^{-3}$ at growth temperature [8–10]. As no carbon-containing compounds were detected by XRD, the incorporation behavior of carbon remains unclear; however, a solubility limit exceeding $10^{20}\,cm^{-3}$ is predicted by calculations [17].

## 4. Electrical, optical and thermal properties

### 4.1. Electrical resistivity

Electrical resistivity was measured in van-der-Pauw geometry at temperatures ranging from 293 K up to 700 K on a suitable single-crystalline area of the first wafer counting from the final as-grown surface of an ingot from series B. Four contacts (contact distance 1.0 mm, square formation) were fabricated on the surface of the wafer using Ti deposition by electron beam evaporation and subsequent annealing at 600°C in vacuum for 5 min. While the sample is electrically insulating at room temperature and no value could be obtained, the resistivity at 500 K is measured to be about $2 \times 10^7\,\Omega cm$. The resistivity decreases with temperature exhibiting a thermal activation energy of about 860 meV in the 500–650 K range as shown in Fig. 4. Li and Tansley [25] found an activation energy of 790 meV and a resistivity of $3 \times 10^{13}\,\Omega cm$ at room temperature on thin AlN films fabricated by CVD. Tansley and Egan [26] assigned this conductivity to nitrogen vacancies $V_N$, for which a ground state 900 meV below the conduction band was calculated. As our results extrapolate to $2.1 \times 10^{13}\,\Omega cm$ at 293 K and thermal activation energies are comparable, the origin of conductivity in our case may be similar to the case of CVD films. Unfortunately, other samples from both series A and B did not allow for comparable single-grain measurements.

### 4.2. Optical absorption

Optical absorption was measured on polished AlN wafers to further investigate electronic properties. Optical absorption was investigated at room temperature in the 200–3200 nm wavelength range (i.e. photon energies ranging from 0.4 to 6.2 eV) on a Perkin–Elmer Lambda 19 spectrometer with an illumination spot size of about 1 mm × 3 mm. The spot size allowed for single-grain measurements on wafers from series B, whereas the grains size of wafers from series A led to 'multi-grain measurements'. The spectra were corrected for single reflections taking into

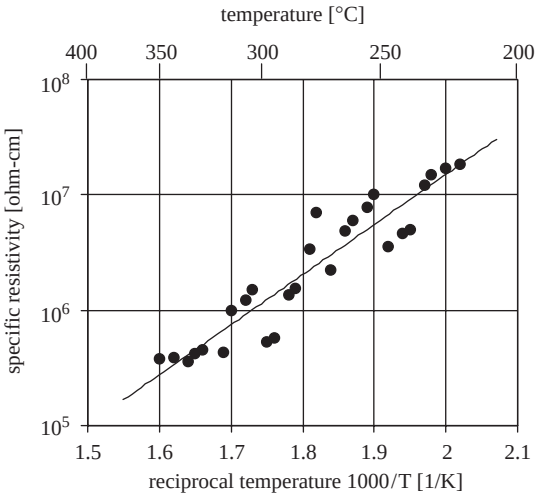


Fig. 4. Temperature dependence of the resistivity of an AlN sample from series B.

account the wavelength-dependent refractive index published by Pastrnak and Roskovcova [27].

Generally, the samples are inhomogeneous in respect to their optical properties (see also Fig. 3). In several wafers measured at over 20 randomly selected areas, the background absorption can deviate up to about 20%. In the polycrystalline samples, impurity incorporation and defect density of the investigated grains can depend on crystal orientation and polarity [2]. Additionally, grain boundaries may lead to increased background absorption. Thus, utmost care was taken to perform the measurements on selected areas of highest and homogeneous optical transmission. Results are shown in Fig. 5.

In all samples, absorption coefficients in the near infrared from 0.4 to 1.5 eV are constant at values as low as 1.5 $cm^{-1}$. No traces of free carrier absorption were found in correspondence to the electrically insulating behavior of the AlN samples. Below the onset of fundamental absorption at energies higher than 5.8 eV (see also Ref. [8,28–31]), homogeneously broadened absorption bands were observed. A band at around 2.8 eV was detected in all of our samples. This band is responsible for the yellowish color of the AlN crystals; it is typically stronger in the samples from series B. The strength and appearance of additional bands in the 3.0–5.8 eV energy range is dependent on growth temperature (series A vs. series B) as well as on the position the sample was cut out from the boule. In wafers from series A, absorption rises continuously in the 3.0–5.8 eV energy range. Up to four absorption shoulders at around 4.4, 4.75, 5.0 and 5.6 eV can be identified. Contrary, in wafers from series B, only a single broad band shows up, peaking in the energy range of 3.8–4.4 eV. Although the band is extended towards higher photon energies presumably caused by accompanying shoulders, generally absorption is lower in the 5.0–5.8 eV range as compared to samples from series A. Measurements performed at 13 K have shown that optical absorption does not change significantly with temperature. Thus, we attribute the observed features to photoionization of deep donor electrons, as the occupation of neutral deep levels is virtually independent on temperature in the investigated range.

Optical absorption is typically decreasing from wafers cut from near the seeding layer to wafers near the final as-grown surface as shown in Fig. 5. The high background absorption in the samples cut from near the seeding layer can be attributed to

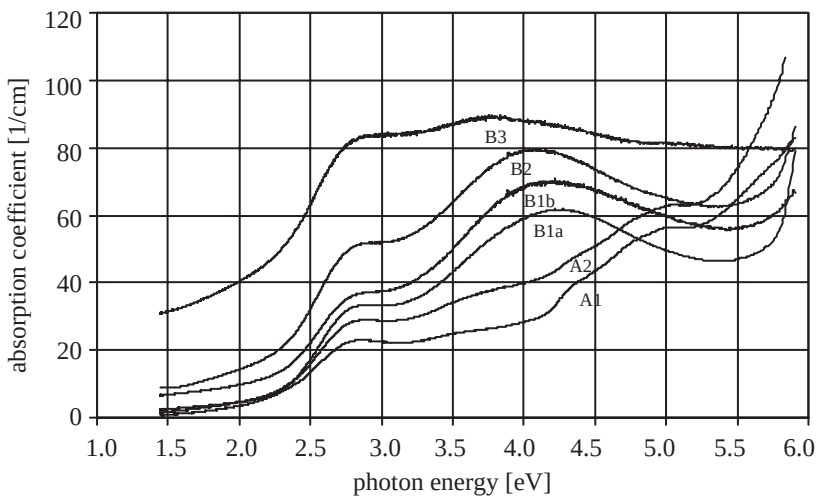


Fig. 5. Optical absorption spectra (visible/UV range) of AlN samples. Sample notation is as follows: the capital letter denotes the growth series (see text), the number indicates the position the sample was cut from the boule (1: near the final as-grown surface of the boule, 2: middle region, 3: near the seeding layer). For sample B1, two absorption curves are shown (B1a and B1b), which were measured at different positions on the sample.

a combination of: (i) the presence of many grain boundaries in the seeding layer, (ii) enhanced incorporation of impurities at early stages of growth, and (iii) pronounced misorientation of the grains at early stages of growth leading to increased defect density and/or impurity incorporation. But even if background absorption is subtracted from the spectra, a decrease in strength of all absorption bands is observed as the sample position moves from near the seeding layer to the as-grown surface of the boule. Thus we assume that the bands are either caused by impurities acting as finite sources, i.e. decreasing contamination during growth, or by defects forming in higher concentrations at early stages of growth. Additionally, the absorption band in the 3.8–4.4 eV energy range gets narrower and its position shifts toward higher energies. This shift is, however, significant only in samples from series B.

Chemical analysis alone is not sufficient to unambiguously assign observed absorption bands to certain defects. Furthermore, knowledge of transient impurity incorporation and defect formation in our process is lacking. We can only tentatively assume that tungsten contamination may increase with increasing temperature, and tungsten coming from the crucible may act as infinite source. Contrary, oxygen presumably acts as finite source, as oxygen contamination is limited by the content within the starting material that is released mostly at early stages of growth. Finally, it is assumed in literature [1] that the concentration of nitrogen vacancies $V_N$ increases with increasing growth temperature.

AlN absorption spectra published in literature are manifold and varying, and so are the tentative assignments of the observed bands to certain defects. Thus, we will briefly discuss those assignments in relation to our findings in order to find out which defects may have significant impact on the properties of our material.

It has been proposed in literature that the absorption band at 2.8 eV is caused by aluminum excess, i.e. nitrogen deficiency, in the lattice [2,8,32]. However, the ionization levels calculated for $V_N$ [26,33] do not fit, and no agreed model exists on how those vacancies would lead to the absorption band observed. For interstitial aluminum as proposed by Cox et al. [32], no data are available. According to our chemical analysis, the peak may be attributed to tungsten contamination. Slack and McNelly, however, have observed the same band also in AlN grown in rhenium crucibles [1]. Finally, the band is presumably not correlated to oxygen, in correspondence to suggestions of Slack et al. [2,8]. Its nature hence remains unclear.

Absorption features in the 3.5–5.0 eV range are commonly designated as 'oxygen related' in literature. Pastrnak and Roskovcova [29] investigated optical absorption in highly contaminated AlN platelets grown by direct reaction of aluminum vapor with nitrogen at 1900°C. Their samples showed absorption bands at 4.5 and 4.8 eV, of which the strength is directly correlated to oxygen content. Assuming that oxygen acts as finite source, i.e. oxygen contamination decreases during growth, our results for samples from series A fit well to this scheme. The bands observed in samples from series B, however, cannot be explained in this manner.

Following Slack et al. [8], the oxygen content can be estimated by both position and absorption coefficient of the peak maximum. That way, the oxygen content in our samples from series B was calculated from the 4.2 eV peak to be in the range of $1 \times 10^{19}\,\mathrm{cm}^{-3}$ (following peak position) or $1 \times 10^{20}\,\mathrm{cm}^{-3}$ (following absorption value). Assuming again that oxygen acts as finite source, the decreasing absorption values roughly fit the model proposed by Slack et al. [8], whereas the shift in the position toward higher energies is opposing it. Selecting the 4.4 eV shoulder found in the samples from series A, the oxygen content in these samples was calculated to be about $5 \times 10^{19}\,\mathrm{cm}^{-3}$ both from peak intensity and position. However, Slack's model does not account for the other bands observed in the samples from series A. It should be noted, that the samples discussed in Refs. [1,2,8] were typically grown at temperatures of 2200–2300°C, i.e. higher temperatures as we used for growing samples of series A.

As a summary, samples from series A fit well in the scheme by Pastrnak and Roskovcova [29], while absorption bands of samples from series B

look more similar to the ones presented by Slack et al. [8]. Comparing the samples these research groups have investigated, we find that they strongly differ in both oxygen contamination and growth temperature. In our samples, however, oxygen contamination was comparable, but growth temperature was different. We conclude that growth temperature indeed has a strong impact on optical absorption in the 3.8–5.0 eV range. Possible mechanisms leading to formation of different absorption bands include a shift of the Fermi level and temperature-dependent formation of intrinsic defects.

The 5.0 and 5.6 eV bands are observed in the samples from series A but not in the samples from series B. Bands in this energy area are commonly observed in AlN epilayers [28,31,32,34,35]. Several authors have attributed them to nitrogen vacancies $V_N$. As an example, Zarwasch et al. [35] observed an absorption shoulder in the 4.5–5.5 eV region in sputter-deposited films using a high $Ar/N_2$ ratio and attributed this band to deviations of coordination number. However, the impurity content of the samples investigated in these publications is unclear. Tansley and Egan [26] associate a donor triplet with energies of 900, 390 and 170 meV below the conduction band to $V_N$. This would roughly fit our data assuming that a third peak at about 5.9 eV is concealed by the onset of fundamental absorption. Thus we suggest that absorption bands observed in the 5.0–6.0 eV range in samples from series A are caused by the presence of nitrogen vacancies. The fact that these bands do not show up in samples from series B could be explained again by a shift of the Fermi level or the presence/absence of deep levels which prevent electron transitions from/to the $V_N$ donor levels. Finally, as no correlation between these bands and the 2.8 eV feature is observed, we suggest that the band at 2.8 eV is not caused by nitrogen vacancies.

### 4.3. Thermal conductivity

It is known that even very small amounts of oxygen drastically reduce the thermal conductivity of AlN [8,9,36–38]. This is true even for polycrystalline samples as grain boundary scattering of phonons can be neglected at room temperature and above [38].

Thermal diffusivity $\alpha$ in the 293–1573 K temperature range was determined using the laser-flash method [39,40] on graphite-coated AlN wafers from both series A and series B. The samples were carefully selected to be comparable to the samples used for optical absorption measurements (cf. Section 4.2). The density of every sample was measured at room temperature. As only values in the range of $3.22 \pm 0.1\ g/cm^3$ were measured, the presence of macroscopic voids can be excluded. Thermal conductivity $\lambda$ was calculated from $\alpha$ using temperature-dependent specific heat capacity data published by Bruls et al. [41]. Results are shown in Fig. 6 together with data published by Slack [37] for a bulk AlN sample W201 with about 400 ppm wt oxygen and about 50 ppm wt tungsten content.

In the investigated temperature range, thermal conductivity decreases with rising temperature approximately as $\lambda = \beta/T$, a dependence common for limitation by phonon-phonon scattering [42]. Interestingly, the constant $\beta$ is different for samples grown at different temperatures and varies also with the position the sample was cut from the boule. The value of $\beta$—and thus the value of $\lambda$ at a given temperature—is higher for samples from series A as compared to samples from series B. Additionally, $\beta$ increases for different samples of series B as the sample position moves from near the seeding layer to the final as-grown surface of the boule. As a remark, the $\lambda(T)$ dependence can also be described as $\lambda \propto T^{-\varepsilon}$, leading to the same conclusions as discussed above. Values of $\beta$ and $\varepsilon$ for the different samples are also listed in Fig. 6. It should be noted, that Slack [37] found different temperature dependence ($\lambda \propto T^{-1.25}$) for temperatures above 500 K and higher thermal conductivity at room temperature (285 W/mK) in his sample W201 as compared to our samples. Slack [37] also calculated $\varepsilon = 1.69$ for pure AlN; our samples, however, exhibit values for $\varepsilon$ in the range of 0.84–1.11.

Borom et al. [36] and Slack et al. [37,38] have proposed that the thermal conductivity is limited by phonon scattering on metal vacancies $V_{Al}$. These are introduced by oxygen entering the lattice

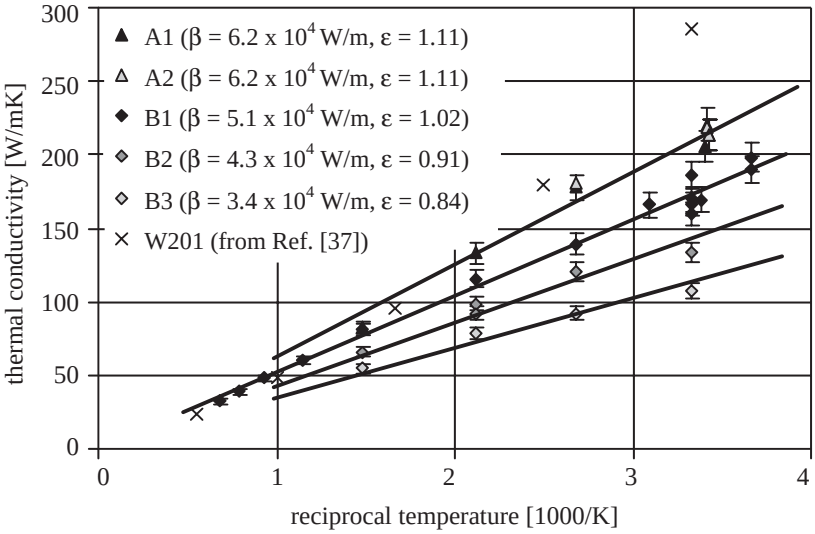


Fig. 6. Temperature dependence of the thermal conductivity of AlN samples. Sample notation is the same as in Fig. 5. Black lines are curves fitting the data points with $\lambda = \beta/T$. Fit parameters $\beta$ and $\varepsilon$ (see text) are given in the legend.

as $Al_2(V_{Al})_1O_3$ groups during growth. Thermal conductivity at room temperature should therefore be linearly correlated to oxygen content [8,38]. Harris et al. [9,10] confirmed these results for AlN ceramics having up to 0.75% at oxygen and proposed that thermal resistance is caused by the defect complex $V_{Al} + O_N$.

Assuming that oxygen contamination decreases during growth, the increase in thermal conductivity as the sample position in the boule moves from near the seeding layer to near the final as-grown surface of the boule can be explained. However, oxygen contamination in our samples from series A and B is comparable (cf. Chapter 3), but thermal conductivity is significantly higher in samples from series A. Yet, there is a striking correspondence between the values for thermal conductivity and the strength of optical absorption in the 2.8–4.5 eV energy range. Samples with higher thermal conductivity at a given temperature show lower absorption coefficients in this energy range. As stated in Chapter 4.2, the absorption in the 3.5–5.0 eV range is designated as 'oxygen-related'; however, our results from optical absorption cannot be explained by oxygen contamination alone. The origin of the band at 2.8 eV is unclear.

We suggest that an increase in growth temperature leads to additional $V_{Al}$ formation and hence to a decrease in thermal conductivity. We also suggest that the absorption bands in the 3.5–5.0 eV energy range are caused by $V_{Al}$, or a combination of $V_{Al}$ and oxygen, rather than oxygen alone. According to Slack et al. [8], $V_N$ and $V_{Al}$ may combine and produce voids, which do not absorb light. This seems to be the case in our samples, as absorption bands attributed to $V_N$ (in the 5.0–5.8 eV energy range) and bands attributed to $V_{Al}$ (in the 3.5–5.0 eV energy range) are anticorrelated. As a remark, the above statements further oppose suggestions that the band at 2.8 eV may be correlated to $V_N$ or interstitial aluminum, as this band is not anticorrelated to absorption bands in the 3.5–5.0 eV energy range.

## 5. Conclusions

We succeeded in the fabrication of AlN crystals with oxygen concentration of about $1 \times 10^{19}\,cm^{-3}$ as measured near the final as-grown surface. This is the lowest oxygen contamination in bulk AlN reported up to date. Comparing samples from boules grown at 2125°C and 2225°C, no increase

of oxygen contamination with growth temperature is observed. Electrical, optical and thermal properties of the samples were analyzed and compared to literature data in order to see (i) by which impurities and defects they are governed and (ii) how they can be further improved. The results can be summarized as follows:

1. The samples are electrically insulating at room temperature. The thermal activation energy of resistivity was measured to be about 860 meV in the 500–650 K range. We attribute this activation energy to nitrogen vacancies, following the analysis of Tansley et al. [25,26] made on CVD films. However, this result awaits verification as only one sample could be measured up to now.
2. In optical absorption, different absorption bands were observed depending on growth temperature and sample position. A band at 2.8 eV was observed in all samples. This band is stronger in samples grown at higher temperature. The origin of this band remains unclear; however, it cannot be attributed to nitrogen vacancies or interstitial aluminum as was suggested in Refs. [2,8,32]. Absorption bands in the 3.5–5.0 eV range cannot be explained by oxygen contamination alone. As oxygen incorporation is accompanied by formation of aluminum vacancies, we suggest that these bands are caused by aluminum vacancies $V_{Al}$, which not only form due to oxygen contamination, but also in temperature-dependent manner. Finally, absorption bands in the 5.0–5.8 eV energy range are attributed to nitrogen vacancies $V_N$. These bands are anticorrelated to the bands caused by aluminum vacancies, which suggests that $V_N$ and $V_{Al}$ may combine and produce voids, which do not absorb light.
3. Thermal conductivity decreases for samples grown at higher temperature and for samples cut from near the seeding layer where oxygen contamination is presumably higher. These results are in full accordance to literature data [36–38] which attribute the decrease in thermal conductivity to the presence of aluminum vacancies.

We conclude that although further reduction of oxygen contamination is considered a key prerequisite for enhancing crystal quality, variations in optical, electrical, and thermal properties, as observed in samples grown at different temperatures, cannot be attributed to oxygen alone. Instead, these properties seem to be governed by formation of vacancies, caused by oxygen or dependent on growth temperature, in samples with low oxygen content. Thus, vacancy formation control is another key issue for further optimization of AlN bulk crystal growth, required especially for substrate use in semiconductor and optoelectronics technology.

## Acknowledgements

The authors would like to thank B. Wiedemann (IKF, University of Frankfurt, Germany) for SSMS measurements, F. Hergert (Chair for Crystallography and Structural Physics, University of Erlangen, Germany) for XRD measurements and analysis, H.-P. Ebert and F. Hemberger (ZAE Bayern, Würzburg/Germany) for laser-flash measurements, and E. Epelbaum for sample preparation. Financial support from the Deutsche Forschungsgemeinschaft (Project no. Wi-393/13) is greatly acknowledged.

## References

[1] G.A. Slack, T.F. McNelly, J. Crystal Growth 34 (1976) 263.
[2] G.A. Slack, T.F. McNelly, J. Crystal Growth 42 (1977) 560.
[3] C.M. Balkas, Z. Sitar, T. Zheleva, L. Bergman, R. Nemanich, R.F. Davis, J. Crystal Growth 179 (1997) 363.
[4] R. Schlesser, R. Dalmau, Z. Sitar, J. Crystal Growth 241 (2002) 416.
[5] J.H. Edgar, L. Liu, B. Liu, D. Zhuang, J. Chaudhuri, M. Kuball, S. Rajasingam, J. Crystal Growth 246 (2002) 187.
[6] Y. Melnik, V. Soukhoveev, V. Ivantsov, V. Sizov, A. Pechnikov, K. Tsvetkov, O. Kovalenkov, V. Dmitriev, A. Nikolaev, N. Kuznetsov, E. Silveira, J. Freitas Jr., Phys. Stat. Sol. (A) 200 (2003) 22.
[7] L.J. Schowalter, G.A. Slack, J.B. Whitlock, K. Morgan, S.B. Shujman, B. Raghothamachar, M. Dudley, K.R. Evans, Phys. Stat. Sol. (C) 0 (2003) 1997.
[8] G.A. Slack, L.J. Schowalter, D. Morelli, J.A. Freitas Jr., J. Crystal Growth 246 (2002) 287.

[9] J.H. Harris, R.A. Youngman, R.G. Teller, J. Mater. Res. 5 (1990) 1763.
[10] R.A. Youngman, J.H. Harris, J. Am. Ceram. Soc. 73 (1990) 3238.
[11] J.W. McCauley, N.D. Corbin, J. Am. Ceram. Soc. 62 (1979) 476.
[12] I. Adams, T.R. AuCoin, G.A. Wolff, J. Electrochem. Soc. 109 (1962) 1050.
[13] K.H. Jack, J. Mater. Sci. 11 (1976) 1135.
[14] F.S. Ohuchi, R.H. French, J. Vac. Sci. Technol. 6 (1988) 1695.
[15] S.F. Bartram, G.A. Slack, Acta Crystallogr. B 35 (1979) 2281.
[16] W. Rafaniello, I.B. Cutler, J. Am. Ceram. Soc. 64 (1981) C–128.
[17] P. Boguslawski, E.L. Briggs, J. Bernholc, Appl. Phys. Lett. 69 (1996) 233.
[18] P. Boguslawski, J. Bernholc, Phys. Rev. B 56 (1997) 9496.
[19] C. Stampfl, J. Neugebauer, C.G. Van de Walle, Mater. Sci. Eng. B 59 (1999) 253.
[20] T. Yamamoto, H. Katayama-Yoshida, Physica B 273–274 (1999) 113.
[21] K. Wongchotigul, N. Chen, D.P. Zhang, X. Tang, M.G. Spencer, Mater. Lett. 26 (1996) 223.
[22] M. Okamoto, Y.K. Yap, M. Yoshimura, Y. Mori, T. Sasaki, Diam. Relat. Mater. 10 (2001) 1322.
[23] D.L. Barrett, R.G. Seidensticker, W. Gaida, R.H. Hopkins, W.C. Choyke, J. Crystal Growth 109 (1991) 17.
[24] G.A. Slack, Mater. Res. Soc. Symp. Proc. 512 (1998) 35.
[25] X. Li, T.L. Tansley, J. Appl. Phys. 68 (1990) 5369.
[26] T.L. Tansley, R.J. Egan, Phys. Rev. B 45 (1992) 10942.
[27] J. Pastrnak, L. Roskovcova, Phys. Stat. Sol. 14 (1966) K5.
[28] W.M. Yim, E.J. Stofko, P.J. Zanzucchi, J.I. Pankove, M. Ettenberg, S.L. Gilbert, J. Appl. Phys. 44 (1973) 292.
[29] J. Pastrnak, L. Roskovcova, Phys. Stat. Sol. 26 (1968) 591.
[30] P.B. Perry, R.F. Rutz, Appl. Phys. Lett. 33 (1978) 319.
[31] M. Morita, K. Tsubouchi, N. Mikoshiba, Jpn. J. Appl. Phys. 21 (1982) 1102.
[32] G.A. Cox, D.O. Cummins, K. Kawabe, R.H. Tredgold, J. Phys. Chem. Solids 28 (1967) 543.
[33] T. Mattila, R.M. Nieminen, Phys. Rev. B 54 (1996) 16676.
[34] C.R. Aita, C.J.G. Kubiak, F.Y.H. Shih, J. Appl. Phys. 66 (1989) 4360.
[35] R. Zarwasch, E. Rille, H.K. Pulker, J. Appl. Phys. 71 (1992) 5275.
[36] M.P. Borom, G.A. Slack, J.W. Szymaszek, Am. Ceram. Soc. Bull. 51 (1972) 852.
[37] G.A. Slack, J. Phys. Chem. Solids 34 (1973) 321.
[38] G.A. Slack, R.A. Tanzilli, R.O. Pohl, J.W. Vandersande, J. Phys. Chem. Solids 48 (1987) 641–647.
[39] J. Hartmann, O. Nilsson, J. Fricke, High Temp. High Press. 25 (1993) 403.
[40] O. Nilsson, H. Mehling, R. Horn, J. Fricke, R. Hofmann, S.G. Müller, R. Eckstein, D. Hofmann, High Temp. High Press. 29 (1997) 73.
[41] R.J. Bruls, H.T. Hintzen, G. de Wirth, R. Metselaar, J.C. van Miltenburg, J. Phys. Chem. Solids 62 (2001) 783.
[42] C. Kittel, Introduction to Solid State Physics, 6th Edition, Wiley, New York, 1986 (chapter 5).